

# LGPCConv: Learnable Gaussian Perturbation Convolution for Lightweight Pansharpening

Chen-Yu Zhao<sup>1</sup>, Tian-Jing Zhang<sup>2</sup>, Ran Ran<sup>3</sup> and Zhi-Xuan Chen<sup>4</sup> and Liang-Jian Deng<sup>\*</sup>

University of Electronic Science and Technology of China, Chengdu, 611731

chenyuzhaouestc@gmail.com, zhangtianjinguestc@163.com, {ranran, 2019050305012}@std.uestc.edu.cn, liangjian.deng@uestc.edu.cn

## Abstract

Pansharpening is a crucial and challenging task that aims to obtain a high spatial resolution image by merging a multispectral (MS) image and a panchromatic (PAN) image. Current methods use CNNs with standard convolution, but we’ve observed strong correlation among channel dimensions in the kernel, leading to computational burden and redundancy. To address this, we propose Learnable Gaussian Perturbation Convolution (LGPCConv), surpassing standard convolution. LGPCConv leverages two properties of standard convolution kernels: 1) correlations within channels, learning a premier kernel as a base to reduce parameters and training difficulties caused by redundancy; 2) introducing Gaussian noise perturbations to simulate randomness and enhance nonlinear representation within channels. We incorporate LGPCConv into a well-designed pansharpening network and demonstrate its superiority through extensive experiments, achieving state-of-the-art performance with minimal parameters (27K). Code is available on the GitHub page of the authors.

## 1 Introduction

With the rapid development of satellite sensors, remote sensing images have become widely used in many fields, *i.e.*, classification, super-resolution, pansharpening, and so on. However, because of the physical limitations of remote sensing imaging devices, images with high spatial and spectral resolutions are hard to achieve by a single sensor. The most typical solution is to make a trade-off between the spatial and spectral resolutions. Therefore, pansharpening, which aims at fusing a low resolution multispectral (LR-MS) image and panchromatic (PAN) data and yielding a high spatial resolution MS image (HR-MS), has become a fundamental task in remote sensing image processing.

This work is supported by NSFC (12271083) and Natural Science Foundation of Sichuan Province (2022NSFSC0501).

\* The corresponding author: Liang-Jian Deng

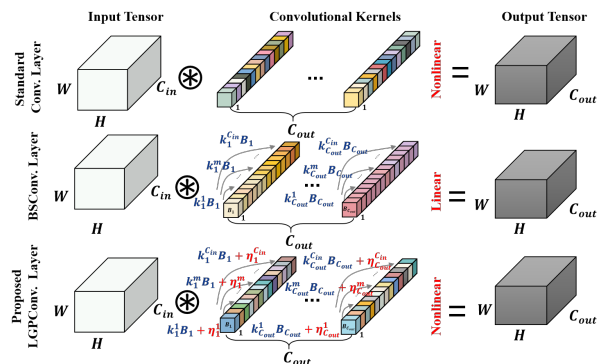


Figure 1: First row: Standard convolution kernels are nonlinear among channels (shown by different colors) but have redundancy (see Fig. 2). Second row: [Haase and Amthor2020] proposed Blueprint Separable Convolution (BSCConv) to reduce parameters. However, its kernels are linear among channels (shown by specific color categories, *i.e.*, yellow and pink), limiting feature representation. Third row: Learnable Gaussian Perturbation Convolution (LGPCConv) uses perturbation to make kernels nonlinear while analyzing correlations among channels. Also, ours has fewer parameters than standard convolution.

Many research efforts have been donated to pansharpening, which can be divided into four groups, *i.e.*, component substitution (CS), multiresolution analysis (MRA), variational optimization (VO), and deep learning (DL) based methods. A detailed review can be found in [Vivone *et al.*2020]. However, the first three methods restrict performance and optimization. With the advancements of hardware in image processing applications, DL-based methods, particularly convolution neural networks (CNNs)-based techniques, are emerging lines of pansharpening [Guo *et al.*2020a, Yang *et al.*2020, T.-J. Zhang and Vivone2022, Jin *et al.*2022b, Zhou *et al.*2022, Yan *et al.*2022a]. However, these DL-based methods often acquire a large number of parameters and suffer from high computational costs and low efficiency.

CNNs have achieved state-of-the-art (SOTA) in many image restoration tasks such as super-resolution, denoising, and pansharpening. The standard convolution focuses on feature extraction and correlation between spatial and channel dimensions. However, the number of parameters of existing convolu-

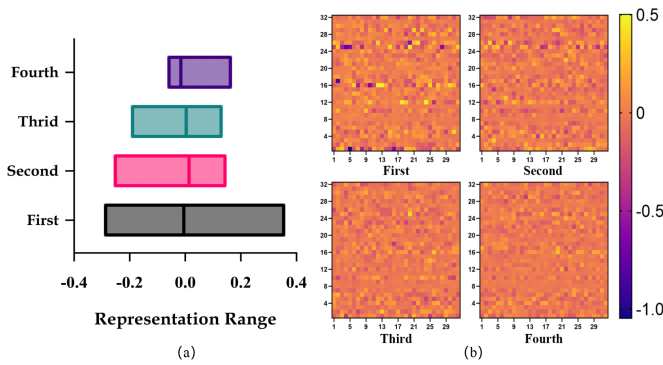


Figure 2: Analysis of correlation among channels of standard convolution kernels. We reshape the standard convolution kernel size from  $32 \times 3 \times 3 \times 32$  to  $32 \times 4 \times 32$  using PCA for the analysis. (a) The principal components of the standard convolution kernel. The vertical axis denotes the first four principal components after PCA, and the horizontal axis represents the representation range of the kernel. (b) The visualized results of the first four principal components of the standard convolution kernel. In each subfigure, the closer two colors, the greater the similarity among channels. This observation indicates the redundancy in the standard convolution kernel.

tion kernels depends on the number of channels of the target feature map. The correlation among channels often makes the convolution kernels redundant. In order to improve the performance and reduce redundancy, many previous attempts have tried to address these issues and have obtained relatively good performances. MobileNets [Howard *et al.*2017] proposed a lightweight structure called a depthwise separable convolution (DSC) module. The DSC module factorizes a standard convolution into a depthwise convolution and a pointwise convolution. In 2020, Hasse *et al.* [Haase and Amthor2020] exploited high redundancy in DSC by visualizing the learned filter kernels, which showed intra-kernel correlations along the depth axis of convolution kernels. Thus, they proposed blueprint separable convolutions (BSConv) with a “blueprint” convolution kernel to generate the whole one and cut down the parameters successfully. However, BSConv has limited representation capability due to its ease of transformation (see Fig. 1 and Fig. 3). For more reviews, please see related works. The main contributions of this paper can be summarized as follows:

- We propose a novel generation of convolution kernels based on channel-wise linear transformation of kernels and noise perturbation bias, namely LGPConv, which uses randomness of noise to achieve kernel nonlinearity. It provides high efficiency for feature representation and facilitates network training with small parameters.
- Using linear algebra, we conduct an in-depth analysis of the unnecessary redundancy caused by the original kernel generation and demonstrate the latent correlation and difference among convolution kernel channels. In addition, we theoretically prove LGPConv’s convergence and explain its implementation in detail.

- Comprehensive analysis on pansharpening performance of our method is conducted through ablation studies, qualitative and quantitative results. Also, to the best of our knowledge, the proposed method can achieve SOTA performance with a small parameter scale (only 27K).

## 2 Related Works and Motivations

### 2.1 CNNs for Pansharpening

As one of the DL-based methods for pansharpening, CNNs have been widely applied in this area by virtue of their powerful nonlinear fitting capabilities. In 2016, Masi *et al.* [Masi *et al.*2016a] pioneered the use of a stacked three-layer convolution network, named PNN, to solve the pansharpening problem, achieving satisfactory results. In the follow-up CNN-based works, researchers have studied from different perspectives, including residual networks [Yang *et al.*2017, Fu *et al.*2020], high-pass filtering details [Yang *et al.*2017, Fu *et al.*2020], multiscale pyramid structure [Yuan *et al.*2018, Jin *et al.*2022a], and bidirectional fusion [Zhang *et al.*2019] to establish a CNN with superior performance to continuously refresh the fusion results of pansharpening. In 2019, Zhuang *et al.* [Zhuang *et al.*2019] developed a method with gradient domain guided image filtering. In order to establish the posterior probability model, [Guo *et al.*2020b] used Bayesian theory to address the pansharpening problem. Furthermore, Deng *et al.* [Deng *et al.*2021] proposed a simple and efficient deep learning network based on traditional CS and MRA method, attaining the current SOTA performance. [Cao *et al.*2022] improved the interpretability. and [Yan *et al.*2022b] combined model-driven and data-driven approaches to design the network.

In general, the existing framework of pansharpening using CNNs can be uniformly expressed as  $\mathcal{F}(\cdot; \theta)$ , where  $\theta$  is the parameters of CNNs. Thus the process can be described as,

$$\widetilde{\mathbf{M}} = \mathbf{M}\uparrow_S + \mathcal{F}(\mathbf{P}, \mathbf{M}\uparrow_S; \theta), \quad (1)$$

where  $\widetilde{\mathbf{M}} \in \mathbb{R}^{H \times W \times C}$  is the fusion of PAN and LR-MS,  $\mathbf{M}\uparrow_S \in \mathbb{R}^{H \times W \times C}$  is the pre-upsampled MS, and  $\mathbf{P} \in \mathbb{R}^{H \times W \times 1}$  denotes the high-resolution (HR) PAN image.

However, the general trend of pansharpening has been to make deeper and more complicated networks without thinking about improving efficiency. Besides, they also ignore the correlations lying in the channel dimension of kernels, which leads to a lot of parameters and duplication that isn’t necessary.

### 2.2 The Standard Convolution and BSConv

**The standard convolution.** The convolution is mainly to use a set of kernels with the size of  $C_{out} \times K \times K \times C_{in}$  to convert an input  $\mathbf{X} = [\mathbf{x}_1, \mathbf{x}_2, \dots, \mathbf{x}_{C_{in}}] \in \mathbb{R}^{H \times W \times C_{in}}$  to an output  $\mathbf{Y} = [\mathbf{y}_1, \mathbf{y}_2, \dots, \mathbf{y}_{C_{out}}] \in \mathbb{R}^{H \times W \times C_{out}}$ , where  $K$  is the kernel size, and  $C_{in}$  and  $C_{out}$  denote the number of the input and the output channels, respectively. Since the output is determined by a group of kernel sets  $\mathbf{W} = [\mathbf{w}_1, \mathbf{w}_2, \dots, \mathbf{w}_{C_{out}}] \in \mathbb{R}^{C_{out} \times K \times K \times C_{in}}$ , where  $\mathbf{w}_i$

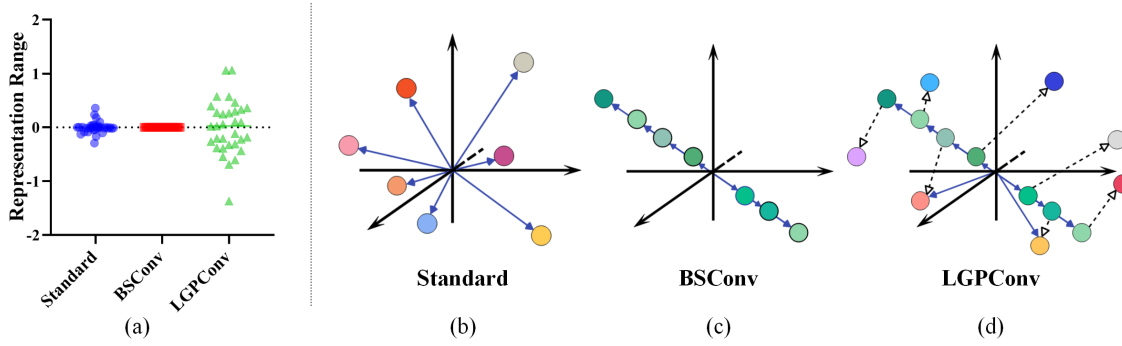


Figure 3: The representation ability of standard convolution, BSConv [Haase and Amthor2020], and the proposed LGPConv through PCA. (a) The representation range shows that the proposed LGPConv has the best represent ability. (b) The standard convolution kernel with size  $K \times K \times C_{in}$  is reshaped to  $C_{in}$  kernel vectors with size  $K^2 \times 1$  according to Def. 3. We set  $C_{in} = 7$  and  $K^2 = 3$  for easier illustration in  $\mathbb{R}^3$  space. The kernel vectors of standard convolution are distributed in  $\mathbb{R}^3$  space. (c) The kernel vectors of BSConv [Haase and Amthor2020] are linear correlated, which can only span a subspace of  $\mathbb{R}^3$  space. This observation motivates us to add some perturbation to make it nonlinear correlated. (d) LGPKernel is distributed in  $\mathbb{R}^3$  space, resulting in high representation ability. The dotted lines stand for the Gaussian Perturbation.

is the  $i^{th}$  set of kernels with the size  $C_{in}$ , the output feature map of  $i^{th}$  channel can be expressed as,

$$\mathbf{y}_i = \mathbf{w}_i * \mathbf{X} = \sum_{m=1}^{C_{in}} w_i^m * \mathbf{x}_m, \quad (2)$$

where  $*$  denotes convolution,  $\mathbf{w}_i = [w_i^1, w_i^2, \dots, w_i^{C_{in}}] \in \mathbb{R}^{K \times K \times C_{in}}$ , and  $\mathbf{x}_m \in \mathbb{R}^{H \times W}$ .

**BSConv.** In BSConv [Haase and Amthor2020], we define each kernel set can be represented by a ‘‘blueprint’’  $\mathbf{B}_i \in \mathbb{R}^{K \times K}$  and the weights  $\mathbf{k}_i = [k_i^1, \dots, k_i^{C_{in}}] \in \mathbb{R}^{C_{in}}$  as follows,

$$\tilde{\mathbf{w}}_i^m = k_i^m \cdot \mathbf{B}_i, \quad (3)$$

where  $\tilde{\mathbf{w}}_i = [\tilde{\mathbf{w}}_i^1, \tilde{\mathbf{w}}_i^2, \dots, \tilde{\mathbf{w}}_i^{C_{in}}] \in \mathbb{R}^{K \times K \times C_{in}}$  is the  $i^{th}$  set of BSConv kernels and  $i \in \{1, \dots, C_{out}\}$ . For BSConv, we rewrite Eq. 2 and Eq. 3 to equivalently get the following pointwise convolution and depthwise convolution,

$$\mathbf{y}'_i = \mathbf{X} * \mathbf{k}_i, \quad (4)$$

$$\mathbf{y}_i = \mathbf{y}'_i * \mathbf{B}_i. \quad (5)$$

Eq. 4 can be seen as a  $1 \times 1$  pointwise convolution with a set of weights  $\mathbf{k}_i$ , while Eq. 5 is a  $K \times K$  depthwise convolution with the ‘‘blueprint’’ kernel  $\mathbf{B}_i$ . Since BSConv [Haase and Amthor2020] utilizes the correlations among channels, it cuts down the parameters from  $C_{out} \times K \times K \times C_{in}$  to  $C_{out} \times (K^2 + C_{in})$ , which achieves the magnificent parameter reduction. However, BSConv can only generate the whole convolution kernel with the linear transformation of the ‘‘blueprint’’ and ignore the nonlinearity among the convolution kernel channels, weakening the convolution’s representation ability.

### 2.3 Motivation

Even though the solutions discussed above have shown promise in solving the pansharpening problem, there is still potential for improvement.

First, the number of learnable parameters increases substantially as the number of layers and channels of convolution

increases in pansharpening problem. But few works in this field focus on lightweight network design, which aims to reduce the scale of parameters by a large amount compared to SOTA approaches. Furthermore, principal component analysis (PCA) demonstrates that not all parameters are fully utilized. Fig. 2 shows that the channels of the standard convolution kernel correlate with each other, resulting in redundancy, which further reduces the efficiency of the network and causes huge computational costs and memory storage.

Second, though BSConv [Haase and Amthor2020] can cut down the parameters by generating a convolution kernel via a ‘‘blueprint’’ and a set of weights, it only has linear representation capability, which restricts the feature extraction ability of BSConv as a general module in CNN. Fig. 3 shows that the BSConv can only span a linear subspace while both the standard convolution and LGPConv are distributed in the whole kernel space.

Third, the above two items motivate us to use the advantage of BSConv to maintain low-scale parameters while taking nonlinearity and randomness into consideration in the design of pansharpening network (see Fig. 1). Since Gaussian distribution is a commonly existing distribution of random variables, it can approximate the probability distribution of the randomness among channels. Thus, generating random perturbations by Gaussian noise is reasonable while considering the correlation among channels.

## 3 Method

### 3.1 Learnable Gaussian Perturbation Convolution

In this section, we propose a novel convolution operation named Learnable Gaussian Perturbation Convolution (LGPConv). To extract key information from feature maps, LGPConv employs the Learnable Gaussian Perturbation Kernel (LGPKernel, see Fig. 1), generated based on the premier ker-

nel (see the following) and noise perturbations. Specifically, the premier kernel is presented as a template considering channel correlations. Furthermore, Gaussian perturbation is used to achieve channel randomization and nonlinear representation.

**The preparation of linear algebra.** To illustrate the given method, we need to first present some basic concepts in linear algebra, which can be found from the book in [Meyer2000].

**Definition 1.** If a set  $\alpha = \{\alpha_1, \dots, \alpha_r\}$  where  $\alpha_i \in \mathbb{R}^n$ , and the  $r$  vectors are independent, then  $\alpha$  can span a subspace  $\mathcal{M}$  of  $\mathbb{R}^n$ .

**Definition 2.** Suppose  $\tilde{\alpha} = \{\tilde{\alpha}_1, \dots, \tilde{\alpha}_m\}$  where  $\tilde{\alpha}_i \in \mathbb{R}^n$ , and all vectors in  $\tilde{\alpha}$  are independent. If  $m \geq r$ , then  $\tilde{\alpha}$  can represent the subspace  $\mathcal{M}$ . Otherwise,  $\tilde{\alpha}$  can not represent the subspace  $\mathcal{M}$ .

**The premier kernel.** As shown in Fig. 2, different channels in a standard kernel have a high degree of correlation, resulting in redundancy and computational inefficiency. The premier kernel, inspired by BSCConv [Haase and Amthor2020], can simplify the kernel of the standard convolution. As shown in Fig. 4, the premier kernel for  $i^{\text{th}}$  output channel mainly composes of a ‘‘blueprint’’ kernel  $\mathbf{B}_i \in \mathbb{R}^{K \times K}$  and a set of corresponding weights  $\mathbf{k}_i \in \mathbb{R}^{C_{in}}$ . Thus, the convolution based on the premier kernel  $\tilde{\mathbf{w}}_i$  can be represented as:

$$\begin{aligned} \mathbf{y}_i &= \sum_{m=1}^{C_{in}} \left( \tilde{\mathbf{w}}_i^m * \mathbf{x}_m \right) = \sum_{m=1}^{C_{in}} \left( \left( \mathbf{k}_i^m \cdot \mathbf{B}_i \right) * \mathbf{x}_m \right) \\ &= \sum_{m=1}^{C_{in}} \underbrace{\left( \underbrace{\left( \mathbf{k}_i^m \cdot \mathbf{x}_m \right)}_{\text{pointwise}} * \mathbf{B}_i \right)}_{\text{depthwise}}, \end{aligned} \quad (6)$$

where  $\mathbf{y}_i$  is  $i^{\text{th}}$  output channel, and  $\mathbf{x}_m, m \in \{1, \dots, C_{in}\}$ , denotes the input tensor. The generation of the premier kernel is two operations in sequence, *i.e.*, pointwise convolution and depthwise convolution. The premier kernel, on the other hand, just analyzes the similarity among channels, ignoring randomness and nonlinearity. In the following, we will give out the relevant mathematical explanations and introduce the solution for the premier kernel’s limitations, *i.e.*, Gaussian perturbation.

**Definition 3.** For easy analysis, we can reshape the  $\mathbf{w}_i \in \mathbb{R}^{K \times K \times C_{in}}$  to  $C_{in}$  vectors  $v_i \in \mathbb{R}^{K^2}$ . The following kernel set is defined as,

$$\mathcal{V} = \left\{ v_i | i = 1, 2, \dots, C_{in}, v_i \in \mathbb{R}^{K^2}, C_{in} \in \mathbb{N} \right\}, \quad (7)$$

where  $v_i$  are distributed as points in  $\mathbb{R}^{K^2}$  space.

Based on Def. 1 and Def. 3, the standard kernel  $\mathbf{w}_i$  with  $K^2$  independent vectors can represent a kernel space  $\mathbb{R}^{K^2}$ . However, the premier kernel  $\tilde{\mathbf{w}}_i$  is linear along the channel dimension. The premier kernel contains  $C_{in}$  points in  $\mathbb{R}^{K^2}$  space (actually located on a line, see an example in Fig. 3 (c)), and is just a subspace of  $\mathbb{R}^{K^2}$ , according to Def. 2.

**Gaussian Perturbation.** The premier kernel only considers the correlation among channels and simplifies the standard kernel by a *linear* transformation, limiting the kernel’s representation capability. To achieve the *nonlinearity* among all

channels, we apply random perturbation to increase randomness, thus expanding the representation range of the premier kernel. Formally, the newly designed kernel is the sum of the premier kernel and the random bias.

$$\begin{aligned} \mathbf{w}_i &= [k_i^1 \cdot \mathbf{B}_i + \eta_i^1, k_i^2 \cdot \mathbf{B}_i + \eta_i^2, \dots, k_i^{C_{in}} \cdot \mathbf{B}_i + \eta_i^{C_{in}}] \\ &= [k_i^1 \cdot \mathbf{B}_i, k_i^2 \cdot \mathbf{B}_i, \dots, k_i^{C_{in}} \cdot \mathbf{B}_i] + [\eta_i^1, \eta_i^2, \dots, \eta_i^{C_{in}}] \\ &= \mathbf{k}_i \cdot \mathbf{B}_i + \eta_i, \end{aligned} \quad (8)$$

where  $\eta_i = [\eta_i^1, \eta_i^2, \dots, \eta_i^{C_{in}}] \in \mathbb{R}^{K \times K \times C_{in}}$  can be viewed as  $C_{in}$  independent vectors with the size of  $K^2 \times 1$  according to Def. 1. Based on Eq. 2 and Eq. 8, we can rewrite the formulation of convolution operation for the  $i$ -th output channel as follows,

$$\begin{aligned} \mathbf{y}_i &= \left( \mathbf{k}_i \cdot \mathbf{B}_i + \eta_i \right) * \mathbf{X} = \sum_{m=1}^{C_{in}} \left( \left( \mathbf{k}_i^m \cdot \mathbf{B}_i + \eta_i^m \right) * \mathbf{x}_m \right) \\ &= \sum_{m=1}^{C_{in}} \left( \left( \mathbf{k}_i^m \cdot \mathbf{x}_m \right) * \mathbf{B}_i + \eta_i^m * \mathbf{x}_m \right). \end{aligned} \quad (9)$$

In the following part, we will demonstrate how to generate  $\eta_i$ . As one type of commonly existing noise, Gaussian noise can produce multiple independent and identically distributed (i.i.d) vectors, which have a probability density function equal to that of the normal distribution. The probability density function  $p$  of a Gaussian random variable  $\epsilon$  is shown as,

$$p_G(\epsilon) = \frac{1}{\sigma\sqrt{2\pi}} \exp\left(-\frac{(\epsilon - \mu)^2}{2\sigma^2}\right), \quad (10)$$

where  $\mu$  and  $\sigma$  are the mean and standard deviation.

Due to the random and independent nature of Gaussian noise, we use it to generate a group of  $\eta_i$ , named *Gaussian perturbation*, see as follows,

$$\eta_i = \mathbf{k}_i \cdot \mathbf{B}_i * \mathcal{H}(\epsilon), \quad (11)$$

where  $\epsilon$  is a tensor of Gaussian random variables and  $\mathcal{H}(\cdot)$  denotes the operations of generating Gaussian perturbation. Given the variety of possible options for  $\mathcal{H}(\cdot)$ , the simplest depthwise and pointwise convolutions in sequence are chosen for cutting down the parameters in this work. Because of the randomness of noise,  $\mathcal{H}(\epsilon)$  can be generated in  $\mathbb{R}^{C_{out} \times K \times K \times C_{in}}$ , which includes multiple independent vectors. Thus, Gaussian perturbation based on  $\eta$  can extend across the entire kernel space.

Though Gaussian perturbation has the same size as the premier kernel, it is independent and random in the kernel space, alleviating the constraints imposed by the linearity of the premier kernel. By injecting Gaussian perturbation into the premier kernel, we obtain the LGPKernel as the following,

$$\mathbf{w}_i = \mathbf{k}_i \cdot \mathbf{B}_i + \eta_i = \mathbf{k}_i \cdot \mathbf{B}_i + \mathbf{k}_i \cdot \mathbf{B}_i * \mathcal{H}(\epsilon). \quad (12)$$

According to Def. 1 and Def. 3, it can be deduced that LGPKernel can represent the kernel space  $\mathbb{R}^{K^2}$  and extract additional rich features.

**Implementation of LGPConv.** To sum up, as Fig. 4 shows, the input feature map is initially extracted using the premier kernel in a convolution process. Then the output is fed into

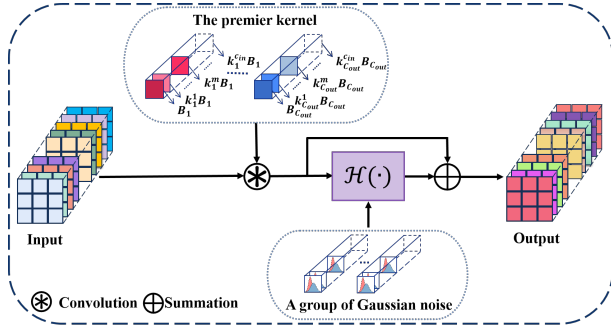


Figure 4: Detailed illustration of the Learnable Gaussian Perturbation Convolution (LGPCConv).

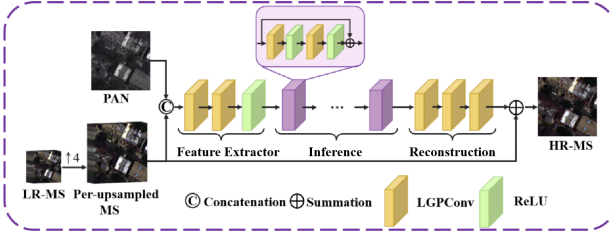


Figure 5: The architecture for LGPCConv-Net. The channel number and details of LGPCConv-Net are specified in supplementary material.

the Gaussian perturbation through convolution operation. Following that, the outputs of two processes (*i.e.*, the convolution based on premier kernel and Gaussian perturbation) are added, and the entire procedure can be summarized as follows,

$$y_i = \sum_{m=1}^{C_{in}} \left( (k_i^m \cdot x_m) * B_i \right) + \sum_{m=1}^{C_{in}} \left( (k_i^m \cdot x_m) * B_i * \mathcal{H}(\epsilon) \right). \quad (13)$$

LGPCConv can reduce parameters from  $C_{out} \times K \times K \times C_{in}$  to  $C_{out} \times (2K^2 + 2C_{in})$  using Eq. 13. See the parameter comparison in Tab. 1.

Convolution Type	Parameters
Standard Conv	$C_{out} \times K \times K \times C_{in}$
BSCConv [Haase and Amthor2020]	$C_{out} \times (K^2 + C_{in})$
LGPCConv	$C_{out} \times (2K^2 + 2C_{in})$

Table 1: The parameters of three convolutions.

### 3.2 Architecture of LGPCConv-based Pansharpening Network (LGPCConv-Net)

We propose the network for pansharpening, *i.e.*, LGPCConv-Net, where all convolutions are realized by LGPCConv. In Fig. 5, the proposed network has three simple components, *i.e.*, an initial feature extractor, a deep inference block, and a fusion reconstruction. More details please see supplementary.

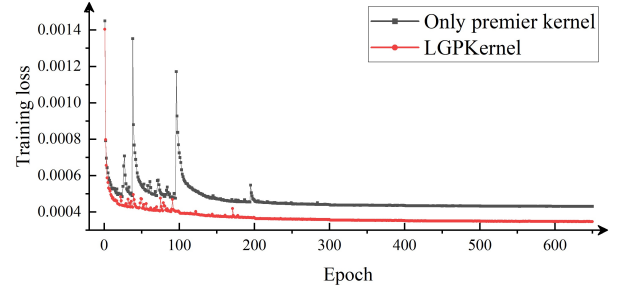


Figure 6: Convergence comparison when using only premier kernel and LGPCKernel.

Training process uses a simple  $\ell_1$  loss to minimize the difference between the predicted image  $\tilde{M}_i$  and the ground truth  $M_{gt,i}$ ,

$$\ell(\theta) = \frac{1}{N} \sum_{i=1}^N \|M_{gt,i} - \tilde{M}_i\|_1, \quad (14)$$

where  $N$  is the sample number, and  $\|\cdot\|_1$  is the  $\ell_1$  norm.

### 3.3 Mathematical Explanations: Convergence Analysis with Lipschitz Condition

Recent research has demonstrated that the Lipschitz constant can be utilized to demonstrate the robustness of DL-based networks [Liu *et al.*2018, Hein and Andriushchenko2017, Weng *et al.*2018]. In this paper, we use it to explain that the training of LGPCConv-Net is equivalent to Lipschitz regularization, which further explains the convergence of the proposed network. The Lipschitz constant of LGPCConv-Net is given as the following definition.

**Definition 4.** For the network with specific perturbation, we define the loss function as  $\ell_\epsilon$  that has a Lipschitz constant  $L_{\ell_\epsilon}$ . Also we have the following inequality,

$$|\ell_\epsilon(\theta) - \ell_\epsilon(\tilde{\theta})| \leq L_{\ell_\epsilon} \|\theta - \tilde{\theta}\|, \quad (15)$$

for network parameters  $\theta$  and  $\tilde{\theta}$ .

Although LGPCConv contains Gaussian perturbation, a theoretical convergence analysis shows it is still robust. Then, we demonstrate that our network can regulate the Lipschitz constant by expanding the expectation function,

$$\begin{aligned} \mathbb{E}_{\epsilon \sim N(\mu, \sigma^2)} \ell_\epsilon(\theta) &= \mathbb{E}_{\epsilon \sim N(\mu, \sigma^2)} \left[ \ell_0(\theta) + \epsilon^T \nabla \ell_0(\theta) + \right. \\ &\quad \left. \frac{1}{2} \epsilon^T \nabla^2 \ell_0(\theta) \epsilon + \dots + \frac{1}{k!} \epsilon^k \nabla^k \ell_0(\theta) + \dots \right] \\ &\approx \mathbb{E}_{\epsilon \sim N(\mu, \sigma^2)} \left[ \ell_0(\theta) + \epsilon^T \nabla \ell_0(\theta) + \frac{1}{2} \epsilon^T \nabla^2 \ell_0(\theta) \epsilon \right]. \end{aligned} \quad (16)$$

In Eq. 16, we employ Taylor expansion at  $\epsilon = 0$  and retain only the second-order term because the variance of Gaussian random variables is relatively small in default. By noticing the Gaussian vector  $\epsilon$  is i.i.d with mean  $\mu$  and the quadratic term is directly dependent on variance of noise and the trace

Method	$SAM(\pm std)\downarrow$	$ERGAS(\pm std)\downarrow$	$SCC(\pm std)\uparrow$	$Q8(\pm std)\uparrow$	Params	GFLOPS	A.T.
BSD [Garzelli <i>et al.</i> 2007]	6.9997±2.8530	5.1670±2.2475	0.8712±0.0798	0.8126±0.1234	-	-	0.0151
MTF_GLP_CBD [Aiazzi <i>et al.</i> 2006]	5.2861±1.9582	4.1627±1.7748	0.8904±0.0698	0.8540±0.1144	-	-	0.0161
CVPR19 [Fu <i>et al.</i> 2019]	5.2058±1.8688	5.1411±2.1191	0.8667±0.0604	0.7927±0.1228	-	-	1.5844
PanNet [Yang <i>et al.</i> 2017]	4.0921±1.2733	2.9524±0.9778	0.9495±0.0461	0.8942±0.1170	83K	0.340	0.0025
PNN [Masi <i>et al.</i> 2016b]	4.0015±1.3292	2.7283±1.0042	0.9515±0.0465	0.9083±0.1122	104K	0.299	0.0011
DiCNN [He <i>et al.</i> 2019]	3.9805±1.3292	2.7367±1.0156	0.9517±0.0472	0.9097±0.1170	47K	0.192	<b>0.0005</b>
DMDNet [Fu <i>et al.</i> 2020]	3.9714±1.2482	2.8572±0.9663	0.9527±0.0447	0.9000±0.1142	100K	0.359	0.0043
FusionNet [Deng <i>et al.</i> 2021]	3.7435±1.2259	2.5679±0.9442	0.9580±0.0450	0.9135±0.1122	79k	0.323	0.0022
LPPN [Jin <i>et al.</i> 2022a]	3.9021±1.2901	2.6404±0.9600	0.9552±0.0450	0.9130±0.1110	51k	1.285	0.0051
LGPCConv-Net	<b>3.5940±1.2141</b>	<b>2.4560±0.9295</b>	<b>0.9596±0.0446</b>	<b>0.9161±0.1107</b>	<b>27K</b>	<b>0.112</b>	0.0034

Table 2: Quantitative comparisons on 1258 samples from WV-3 dataset. (**Bold**: best)

of Hessian, Eq. 16 can be formulated as,

$$\mathbb{E}_{\epsilon \sim N(\mu, \sigma^2)} \ell_\epsilon(\theta) \approx \ell_0(\theta) + \mu \nabla \ell_0(\theta) + \frac{\sigma^2}{2} \text{Tr} \{ \nabla^2 \ell_0(\theta) \}. \quad (17)$$

As a convex relaxation, if we assume  $\ell_0(\theta)$  is convex, then Eq. 17 can be formulated as follows according to Def. 4.,

$$\ell_\epsilon(\theta) \approx \ell_0(\theta) + \left( \mu + \frac{\sigma^2}{2} \right) L \ell_0, \quad (18)$$

which indicates that the training of LGPCConv-Net is equivalent to training the network without perturbation and an extra regularization of the Lipschitz constant. By controlling both mean and variance of Gaussian noise, we can balance the convergence of LGPCConv-Net. The training loss curves for only using the premier kernel and LGPCConv are shown in Fig. 6. It can be observed that huge fluctuations exist when having no Gaussian perturbation (*i.e.*, only premier kernel), while LGPCConv holds a steady loss convergence.

## 4 Experiments

Due to the page limitation, **dataset**, **metrics**, **compared methods**, and **training platform** are mentioned in supplementary.

### 4.1 Assessment on 8-band and 4-band Dataset

In Tab. 2, we show the average quantitative results of different methods on the 1258 samples from WV-3 dataset with eight bands. The proposed LGPCConv-Net clearly has the best performance and the fewest computational costs (parameters and GFLOPS) compared to all other methods simultaneously. Furthermore, we exhibit the average inference time for each fusion method, denoted as *A.T.* in seconds. We also assess the proposed method on 4-band datasets, *i.e.*, GF-2 and QB data. The quantitative results in terms of all compared methods are shown in Tab. 3. As can be seen, LGPCConv-Net outperforms other competing methods with lower *SAM* and *ERGAS* and higher *Q4* and *SCC*, which proves that the proposed LGPCConv-Net can tackle with 4-band dataset efficiently while maintaining the smallest parameter scale. For **visual comparisons**, please refer to supplementary material.

### 4.2 Discussion

**The number of Resnet-like blocks in LGPCConv-Net.** Since we have set the number of Resnet-like blocks ( $N$ ) to 4 in default, the influence of Resnet-like blocks will be demonstrated

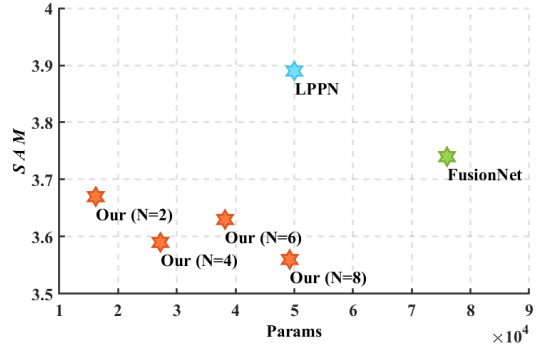


Figure 7: The impact of the number of Resnet-like blocks ( $N$ ). The horizontal axis stands for the parameters that the corresponding networks need.

by justifying its number. We have tested the performance of LGPCConv-Net with the different number of Resnet-like blocks in the deep inference block, where  $N = 2, 4, 6, 8$ . The experiments are only conducted on WV-3 dataset in the discussion. As Fig. 7 shows, all the LGPCConv-Net with varying  $N$  have good performance and all outperform LPPN [Jin *et al.* 2022a] and FusionNet [Deng *et al.* 2021] with less parameters. Though there are fluctuations with  $N$  increasing,  $N = 4$  is an economical choice.

**Gaussian perturbation and Gaussian noise.** In this section, we assess the effectiveness of Gaussian perturbation and the corresponding Gaussian noise in LGPCConv. In order to illustrate this, we design the following three cases to compare and the results are shown in Tab. 4 (the standard error is omitted for page limiting). LGPKernel outperforms the other two by replacing all LGPKernel with the premier kernel and LGPKernel without (w/o) the Gaussian noise. Thus, both Gaussian perturbation and Gaussian noise are indispensable for LGPKernel. **Different convolution types.** Three different convolutional operations, *i.e.*, standard convolution, BSCConv [Haase and Amthor2020], and LGPCConv, are embedded into the proposed network (Fig. 5). Since the parameters of BSCConv are less than LGPCConv, the number of Resnet-like blocks ( $N$ ) is added to 10 for a fair comparison. As shown in Tab. 5, though standard convolution and BSCConv-based network consume

Method	(a) 81 samples from GF-2 dataset				(b) 48 samples from QB dataset				Params
	SAM( $\pm$ std) $\downarrow$	ERGAS( $\pm$ std) $\downarrow$	SCC( $\pm$ std) $\uparrow$	Q4( $\pm$ std) $\uparrow$	SAM( $\pm$ std) $\downarrow$	ERGAS( $\pm$ std) $\downarrow$	SCC( $\pm$ std) $\uparrow$	Q4( $\pm$ std) $\uparrow$	
BSDS [Garzelli <i>et al.</i> 2007]	2.29 $\pm$ 0.66	2.07 $\pm$ 0.61	0.87 $\pm$ 0.05	0.87 $\pm$ 0.04	7.75 $\pm$ 1.93	7.46 $\pm$ 0.99	0.85 $\pm$ 0.06	0.70 $\pm$ 0.12	-
MTF_GLP_CBD [Aiuzzi <i>et al.</i> 2006]	2.26 $\pm$ 0.72	2.02 $\pm$ 0.60	0.87 $\pm$ 0.05	0.87 $\pm$ 0.04	7.67 $\pm$ 1.88	7.42 $\pm$ 0.97	0.85 $\pm$ 0.06	0.65 $\pm$ 0.14	-
CVPR19 [Fu <i>et al.</i> 2019]	2.15 $\pm$ 0.50	2.24 $\pm$ 0.64	0.87 $\pm$ 0.04	0.86 $\pm$ 0.02	7.69 $\pm$ 1.84	9.15 $\pm$ 1.52	0.82 $\pm$ 0.04	0.55 $\pm$ 0.19	-
PanNet [Yang <i>et al.</i> 2017]	1.39 $\pm$ 0.32	1.22 $\pm$ 0.28	0.95 $\pm$ 0.01	0.94 $\pm$ 0.02	5.31 $\pm$ 0.99	5.23 $\pm$ 0.54	0.93 $\pm$ 0.06	0.82 $\pm$ 0.08	78K
PNN [Masi <i>et al.</i> 2016b]	1.45 $\pm$ 0.36	1.27 $\pm$ 0.32	0.94 $\pm$ 0.02	0.94 $\pm$ 0.02	5.20 $\pm$ 0.95	4.87 $\pm$ 0.46	0.93 $\pm$ 0.05	0.83 $\pm$ 0.07	80K
DiCNN [He <i>et al.</i> 2019]	1.49 $\pm$ 0.38	1.32 $\pm$ 0.35	0.94 $\pm$ 0.02	0.94 $\pm$ 0.02	5.30 $\pm$ 0.99	5.23 $\pm$ 0.54	0.92 $\pm$ 0.05	0.81 $\pm$ 0.08	43K
DMDNet [Fu <i>et al.</i> 2020]	1.29 $\pm$ 0.31	1.12 $\pm$ 0.26	0.96 $\pm$ 0.01	0.95 $\pm$ 0.02	5.11 $\pm$ 0.94	4.74 $\pm$ 0.65	0.94 $\pm$ 0.06	0.83 $\pm$ 0.07	98K
FusionNet [Deng <i>et al.</i> 2021]	1.18 $\pm$ 0.27	1.00 $\pm$ 0.22	0.97 $\pm$ 0.01	0.96 $\pm$ 0.01	5.31 $\pm$ 1.02	5.16 $\pm$ 0.68	0.93 $\pm$ 0.05	0.82 $\pm$ 0.08	76k
LPPN [Jin <i>et al.</i> 2022a]	1.34 $\pm$ 0.25	1.05 $\pm$ 0.22	0.96 $\pm$ 0.01	0.96 $\pm$ 0.02	4.84 $\pm$ 0.83	4.61 $\pm$ 0.88	0.95 $\pm$ 0.05	0.84 $\pm$ 0.07	160K
LGPCConv-Net	<b>1.17<math>\pm</math>0.28</b>	<b>0.98<math>\pm</math>0.24</b>	<b>0.97<math>\pm</math>0.01</b>	<b>0.97<math>\pm</math>0.02</b>	<b>4.42<math>\pm</math>0.74</b>	<b>3.70<math>\pm</math>0.27</b>	<b>0.96<math>\pm</math>0.05</b>	<b>0.86<math>\pm</math>0.06</b>	<b>27K</b>

Table 3: Quantitative comparisons on 81 samples from GF-2 dataset and 48 samples from QB dataset, respectively. (**Bold**: best)

Kernel Type	SAM $\downarrow$	ERGAS $\downarrow$	SCC $\uparrow$	Q8 $\uparrow$
Only premier kernel	4.064	2.796	0.950	0.905
LGPKernel w/o Gaussian noise	3.823	2.607	0.956	0.913
LGPKernel	<b>3.594</b>	<b>2.456</b>	<b>0.961</b>	<b>0.918</b>

Table 4: Quantitative results by replacing all the LGPKernel in LGPCConv-Net with the premier kernel and LGPKernel w/o Gaussian perturbation. (**Bold**: best)

more parameters than LGPCConv, the proposed LGPCConv still obtains the best performance among all. Therefore, LGPCConv has addressed the existing problems for standard convolution and BSConv, *i.e.*, reducing the scale of parameter and enlarging the representation range simultaneously.

Convolution Type	SAM $\downarrow$	ERGAS $\downarrow$	SCC $\uparrow$	Q8 $\uparrow$	N	Params
Standard Conv	3.803	2.593	0.956	0.914	4	87K
BSConv [Haase and Amthor 2020]	3.845	2.857	0.952	0.910	10	29K
LGPCConv	<b>3.594</b>	<b>2.456</b>	<b>0.961</b>	<b>0.918</b>	4	<b>27K</b>

Table 5: Quantitative results with three different types of convolution, *i.e.*, standard convolution, BSConv, and LGPCConv, which are embedded in the same network architecture. (**Bold**: best)

$\sigma_1$	$\sigma_2$	SAM $\downarrow$	ERGAS $\downarrow$	SCC $\uparrow$	Q8 $\uparrow$
0.003	0.005	3.695	2.513	0.959	0.915
0.001	0.005	3.665	2.515	0.959	0.915
0.005	0.003	3.615	2.485	0.960	0.918
0.005	0.001	3.650	2.505	0.960	0.917
0.005	0.005	<b>3.594</b>	<b>2.456</b>	<b>0.961</b>	<b>0.918</b>

Table 6: Quantitative comparisons with different initial Gaussian noise distribution, *i.e.*,  $N(0, \sigma_1^2)$  and  $N(0, \sigma_2^2)$ , for depthwise and pointwise convolutions, respectively. (**Bold**: best)

**The initial distribution of Gaussian noise.** As mentioned in the accomplishment of LGPCConv, Gaussian noise is the key input for generating Gaussian perturbation, and depthwise and pointwise convolutions are used in sequence for parameter reduction. Thus, there are two sets of Gaussian noise for both depthwise and pointwise convolutions. Next, we will examine how the initial distributions, *i.e.*,  $\mu$  and  $\sigma$ , affect the performance of LGPCConv-Net. First, considering the Gaussian noise for depthwise and pointwise convolutions follows

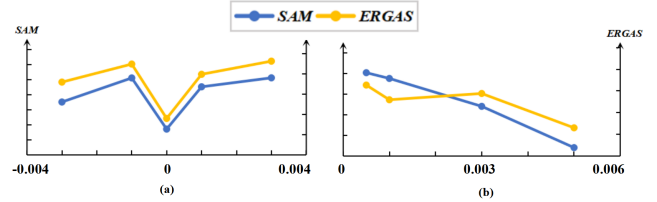


Figure 8: (a) The impact of initial Gaussian distribution with varying mean values. (b) The impact of initial Gaussian distribution with varying standard deviations.

different initial distributions, *i.e.*,  $N(\mu_1, \sigma_1^2)$  and  $N(\mu_2, \sigma_2^2)$ , respectively. For easier analysis, we set the  $\mu_1 = \mu_2 = 0$  as the default. Tab. 6 demonstrates that optimal performance is achieved when the initial distributions are identical. Then, the impact of  $\mu$  and  $\sigma$  will be tested with two sets of Gaussian noise, whose initial distributions are identical. Fig. 8 (a) shows that  $\mu = 0$  has the best outcomes. From Fig. 8 (b), the results have improved with  $\sigma$  increasing, which indicates that the initial distribution of Gaussian noise is valid and our LGPCConv-Net is robust to the perturbation.

## 5 Conclusion

Standard convolution is highly redundant due to the unawareness of channel-across correlations. We propose a novel convolution, *i.e.*, LGPCConv, which consists of the premier kernel and Gaussian perturbation. The premier kernel effectively reduces the parameters by considering the similarity among channels, while Gaussian perturbation promises the randomness and nonlinearity of the LGPKernel. Based on the LGPCConv, a simple end-to-end network, *i.e.*, LGPCConv-Net, is designed for pansharpening task. Extensive experiments show the prominent performance of LGPCConv-Net in terms of quantitative and visual results, while only requiring a very minor scale of parameters to the best of our knowledge. Also, our method has relatively limited generalization, this may be due to Gaussian random perturbation, and it is more sensitive to the distribution changes of datasets acquired by different sensors.

## References

- [Aiazzi *et al.*, 2006] Bruno Aiazzi, L Alparone, Stefano Baronti, Andrea Garzelli, and Massimo Selva. MTF-tailored multiscale fusion of high-resolution ms and pan imagery. *Photogrammetric Engineering & Remote Sensing*, 72(5):591–596, 2006.
- [Cao *et al.*, 2022] Xiangyong Cao, Xueyang Fu, Danfeng Hong, Zongben Xu, and Deyu Meng. Pancsc-net: A model-driven deep unfolding method for pansharpening. *IEEE Transactions on Geoscience and Remote Sensing*, 60:1–13, 2022.
- [Deng *et al.*, 2021] Liang-Jian Deng, Gemine Vivone, Cheng Jin, and Jocelyn Chanussot. Detail injection-based deep convolutional neural networks for pansharpening. *IEEE Transactions on Geoscience and Remote Sensing*, 59(8):6995–7010, 2021.
- [Fu *et al.*, 2019] Xueyang Fu, Zihuang Lin, Yue Huang, and Xinghao Ding. A variational pan-sharpening with local gradient constraints. In *CVPR*, pages 10265–10274, 2019.
- [Fu *et al.*, 2020] Xueyang Fu, Wu Wang, Yue Huang, Xinghao Ding, and John Paisley. Deep multiscale detail networks for multiband spectral image sharpening. *IEEE Transactions on Neural Networks and Learning Systems*, 32(5):2090–2104, 2020.
- [Garzelli *et al.*, 2007] Andrea Garzelli, Filippo Nencini, and Luca Capobianco. Optimal mmse pan sharpening of very high resolution multispectral images. *IEEE Transactions on Geoscience and Remote Sensing*, 46(1):228–236, 2007.
- [Guo *et al.*, 2020a] Penghao Guo, Peixian Zhuang, and Yecai Guo. Bayesian pan-sharpening with multiorder gradient-based deep network constraints. *IEEE Journal of Selected Topics in Applied Earth Observations and Remote Sensing*, 13:950–962, 2020.
- [Guo *et al.*, 2020b] Penghao Guo, Peixian Zhuang, and Yecai Guo. Bayesian pan-sharpening with multiorder gradient-based deep network constraints. *IEEE Journal of Selected Topics in Applied Earth Observations and Remote Sensing*, 13:950–962, 2020.
- [Haase and Amthor, 2020] Daniel Haase and Manuel Amthor. Rethinking depthwise separable convolutions: How intra-kernel correlations lead to improved mobilenets. In *IEEE Conf. Comput. Vis. Pattern Recog. (CVPR)*, pages 14600–14609, 2020.
- [He *et al.*, 2019] Lin He, Yizhou Rao, Jun Li, Jocelyn Chanussot, Antonio Plaza, Jiawei Zhu, and Bo Li. Pansharpening via detail injection based convolutional neural networks. *IEEE Journal of Selected Topics in Applied Earth Observations and Remote Sensing*, 12(4):1188–1204, 2019.
- [Hein and Andriushchenko, 2017] Matthias Hein and Maksym Andriushchenko. Formal guarantees on the robustness of a classifier against adversarial manipulation. In I. Guyon, U. Von Luxburg, S. Bengio, H. Wallach, R. Fergus, S. Vishwanathan, and R. Garnett, editors, *Adv. Neural Inform. Process. Syst. (NIPS)*, volume 30, 2017.
- [Howard *et al.*, 2017] Andrew G Howard, Menglong Zhu, Bo Chen, Dmitry Kalenichenko, Weijun Wang, Tobias Weyand, Marco Andreetto, and Hartwig Adam. Mobilenets: Efficient convolutional neural networks for mobile vision applications. *arXiv preprint arXiv:1704.04861*, 2017.
- [Jin *et al.*, 2022a] Cheng Jin, Liang-Jian Deng, Ting-Zhu Huang, and Gemine Vivone. Laplacian pyramid networks: A new approach for multispectral pansharpening. *Information Fusion*, 78:158–170, 2022.
- [Jin *et al.*, 2022b] Zi-Rong Jin, Tian-Jing Zhang, Tai-Xiang Jiang, Gemine Vivone, and Liang-Jian Deng. Lagconv: Local-context adaptive convolution kernels with global harmonic bias for pansharpening. *AAAI Conference on Artificial Intelligence (AAAI)*, 36(1):1113–1121, 2022.
- [Liu *et al.*, 2018] Xuanqing Liu, Minhao Cheng, Huan Zhang, and Cho-Jui Hsieh. Towards robust neural networks via random self-ensemble. In *ECCV*, pages 369–385, 2018.
- [Masi *et al.*, 2016a] Giuseppe Masi, Davide Cozzolino, Luisa Verdoliva, and Giuseppe Scarpa. Pansharpening by convolutional neural networks. *Remote Sensing*, 8(7):594, 2016.
- [Masi *et al.*, 2016b] Giuseppe Masi, Davide Cozzolino, Luisa Verdoliva, and Giuseppe Scarpa. Pansharpening by convolutional neural networks. *Remote Sensing*, 8(7):594, 2016.
- [Meyer, 2000] Carl Meyer. *Matrix Analysis and Applied Linear Algebra Book and Solutions Manual*. 01 2000.
- [T.-J. Zhang and Vivone, 2022] T.-Z. Huang J. Chanussot T.-J. Zhang, L.-J. Deng and G. Vivone. A triple-double convolutional neural network for panchromatic sharpening. *IEEE Transactions on Neural Networks and Learning Systems*, 2022.
- [Vivone *et al.*, 2020] Gemine Vivone, Mauro Dalla Mura, Andrea Garzelli, Rocco Restaino, Giuseppe Scarpa, Magnus O Ulfarsson, Luciano Alparone, and Jocelyn Chanussot. A new benchmark based on recent advances in multispectral pansharpening: Revisiting pansharpening with classical and emerging pansharpening methods. *IEEE Geoscience and Remote Sensing Magazine*, 9(1):53–81, 2020.
- [Weng *et al.*, 2018] Tsui-Wei Weng, Huan Zhang, Pin-Yu Chen, Jinfeng Yi, Dong Su, Yupeng Gao, Cho-Jui Hsieh, and Luca Daniel. Evaluating the robustness of neural networks: An extreme value theory approach, 2018.
- [Yan *et al.*, 2022a] Keyu Yan, Man Zhou, Jie Huang, Feng Zhao, Chengjun Xie, Chongyi Li, and Danfeng Hong. Panchromatic and multispectral image fusion via alternating reverse filtering network. In Alice H. Oh, Alekh Agarwal, Danielle Belgrave, and Kyunghyun Cho, editors, *Advances in Neural Information Processing Systems*, 2022.



- [Yan *et al.*, 2022b] Yinsong Yan, Junmin Liu, Shuang Xu, Yicheng Wang, and Xiangyong Cao. Md<sup>3</sup>net: Integrating model-driven and data-driven approaches for pansharpening. *IEEE Transactions on Geoscience and Remote Sensing*, 60:1–16, 2022.
- [Yang *et al.*, 2017] Junfeng Yang, Xueyang Fu, Yuwen Hu, Yue Huang, Xinghao Ding, and John Paisley. Pannet: A deep network architecture for pan-sharpening. In *Int. Conf. Comput. Vis. (ICCV)*, pages 5449–5457, 2017.
- [Yang *et al.*, 2020] Yong Yang, Chenxu Wan, Shuying Huang, Hangyuan Lu, and Weiguo Wan. Pansharpening based on low-rank fuzzy fusion and detail supplement. *IEEE Journal of Selected Topics in Applied Earth Observations and Remote Sensing*, 13:5466–5479, 2020.
- [Yuan *et al.*, 2018] Qiangqiang Yuan, Yancong Wei, Xi-angchao Meng, Huanfeng Shen, and Liangpei Zhang. A multiscale and multidepth convolutional neural network for remote sensing imagery pan-sharpening. *IEEE Journal of Selected Topics in Applied Earth Observations and Remote Sensing*, 11(3):978–989, 2018.
- [Zhang *et al.*, 2019] Yongjun Zhang, Chi Liu, Mingwei Sun, and Yangjun Ou. Pan-sharpening using an efficient bidirectional pyramid network. *IEEE Transactions on Geoscience and Remote Sensing*, 57(8):5549–5563, 2019.
- [Zhou *et al.*, 2022] Man Zhou, Jie Huang, Keyu Yan, Hu Yu, Xueyang Fu, Aiping Liu, Xian Wei, and Feng Zhao. Spatial-frequency domain information integration for pan-sharpening. page 274–291, Berlin, Heidelberg, 2022. Springer-Verlag.
- [Zhuang *et al.*, 2019] Peixian Zhuang, Qingshan Liu, and Xinghao Ding. Pan-ggf: A probabilistic method for pansharpening with gradient domain guided image filtering. *Signal Processing*, 156:177–190, 2019.